Modelling the outcomes of high–velocity impacts between small solar system bodies

Jean-Marc Petit

CNRS, Observatoire de Nice, B.P. 229, 06304 Nice Cedex 04, France

Paolo Farinella

Observatoire de Nice, B.P. 229, 06304 Nice Cedex 04, France

Dipartimento di Matematica, Università di Pisa, Via Buonarroti 2, 56127 Pisa, Italy

Abstract

We present a self–consistent numerical algorithm aimed at predicting the outcomes of high–velocity impacts between asteroids (or other small bodies of the solar system), based on a set of model input parameters which can be estimated from the available experimental evidence, and including the possible gravitational reaccumulation of ejected fragments whose velocity is less than a suitably defined escape velocity. All the fragment mass distributions are modelled by truncated power laws, and a possible correlation between fragment ejection velocity and mass is taken into account in different ways, including a probabilistic one. We analyze in particular the effectiveness of the gravitational reaccumulation process in terms of different choices of the collisional parameters and the assumed relationship between fragment speed and mass. Both the transition size beyond which solid targets are likely to reaccumulate a large fraction of the fragment mass and the collision energy needed to disperse most of the fragments are sensitive functions of the assumed fragment velocity versus mass relationship. We also give some examples of how our algorithm can be applied to study the origin and collisional history of small solar system bodies, including the asteroid 951 Gaspra (recently imaged by the Galileo probe) and the asteroid families.

1 Introduction

As a consequence of their non–negligible eccentricities and mutual inclinations, the orbits of most asteroids can occasionally intersect each other, opening the way to the occurrence of high–velocity impacts. A typical main–belt asteroid undergoes collisions with other (normally, much smaller) asteroids at an average velocity of 5.8 km/s and at a rate of the order of $3 \times 10^{-18}\ (R/km)^2 N_{pr}\ yr^{-1}$, where R and N_{pr} are the assumed target radius and number of projectiles (Farinella and Davis, 1992). As a consequence, mutual impacts — whose outcomes range from small–scale cratering events to catastrophic target break–up — have played a crucial role in the evolution of the asteroid belt (the pioneering work in this field dates back to the 50s, e.g. Öpik, 1951, and Piotrowski, 1953; for a recent a review, we refer to Davis *et al.*, 1989). In the 80s it has been also realized that disruptive impacts may have been important in the origin and evolution of other types of small solar system bodies, like some icy satellites of the outer planets (Farinella *et al.*, 1983), the planetary rings (Harris, 1984), and the interplanetary dust complex (Sykes *et al.*, 1989).

In order to model the outcomes of collisional events occurring in the solar system, hyper-velocity impact experiments have been carried out in the laboratory at a much smaller scale (for reviews, see Davis *et al.*, 1986; Fijiwara *et al.*, 1989), and from the observed results some simple empirical relationships have been derived to describe the collisional outcomes in terms of several basic *input parameters*, such as the projectile and target masses, the impact velocity, some coefficients describing the impact response of the target's material, and sometimes the incidence angle (when it is relevant to distinguish between "central" and "grazing" impacts). For the sake of simplicity, both the target and the projectile are normally considered as nearly homogeneous and spherical bodies (see Chapman *et al.*, 1989, for a discussion of possible complications). It is important to keep in mind that at least one physically fundamental difference exists between small laboratory targets and real celestial bodies, which are tens or hundreds of km across: in the latter case, self–gravity is not negligible, and this has two important consequences. First, self–compression can strengthen the interior of the bodies making more difficult to fracture and shatter them, and second — if fragmentation occurs — mutual gravity can cause the partial reaccumulation of the ejected fragments into a so–called *pile of rubble*.

From the theoretical point of view, our understanding of the complex physical processes which take place after an energetic impact is still quite limited. Research work on this subject is currently in progress, based either on semiempirical working hypotheses about the fracture criteria and the geometry of fragment velocity fields (Paolicchi *et al.*, 1989, 1992), or on the integration of suitable hydrodynamical equations in two or three dimensions (Ryan *et al.*, 1990; Ryan and Melosh, 1992; Nolan *et al.*, 1992; Asphaug *et al.*, 1992). However, the corresponding numerical experiments are still so complicated and demanding (in terms of CPU time and memory) that they cannot be used to explore the full range of the relevant parameters, in order to interpolate and extrapolate to actual solar system conditions, nor to simulate the long–term collisional evolution of systems like the asteroid belt or the planetary rings. Therefore, the results of both the laboratory and the numerical experiments need to be incorporated into suitable scaling algorithms, requiring a number of input parameters (which depend on the "initial conditions" of the impact and the detailed physical processes following it) and capable of predicting in a fast and effective manner the outcome of any possible impact occurring in the system under scrutiny.

In this paper (Secs. 2 to 5) we present such a numerical algorithm, which is physically simple (but still fully self–consistent) and at the same time fairly realistic, as it includes models for the effects of self–gravity and fragment reaccumulation. This algorithm is a follow–up and a refinement of those used in the past by Greenberg *et al.* (1978), Davis *et al.* (1979, 1985, 1989), and Farinella *et al.* (1992), as it includes some additional physical effects. In Sec. 6 we shall discuss how much the predictions of our algorithm are sensitive to different choices of some collisional parameters, and how the effectiveness of the gravitational reaccumulation process depends upon the assumed relationship between the ejection velocity and the mass of the fragments. We shall also give some examples of how this algorithm can be applied to model the origin of asteroid families and the collisional evolution of different types of small solar system bodies.

2 The fragmentation threshold

In this and the next three sections we are going to describe our algorithm to predict the outcome of a collision between two (spherical and homogeneous) bodies of masses M_i, densities ρ_i, diameters $D_i = (6M_i/\pi\rho_i)^{1/3}$, impact strenghts S_i (the index i is always equal to either 1 or 2), when the relative velocity is V_{rel} and the relative kinetic energy is $E_{rel} = M_1 M_2 V_{rel}^2/2(M_1 + M_2)$. The impact strength S is defined as the mimimum specific energy delivered to each body to cause catastrophic fragmentation of it. We are implicitly assuming that an abrupt transition always occurs between the cratering and shattering regimes. This is supported by the experimental results, which show that the transition from localized target damage to widespread fragmentation is associated with a modest increase of the impact energy (see e.g. Fujiwara *et al.*, 1977, Fig. 10). For targets having a significant self–gravity, recent hydrocode modelling work by Nolan *et al.* (1992) and Greenberg *et al.* (1992) suggests that the transition may be less distinct than indicated by laboratory experiments, in the sense that a very large crater can form and remain on the surface even though a significant fraction of the target material is shattered and reaccumulated. While we shall keep our "catastrophic transition" assumption, we shall treat the formation of giant craters in a way that does not conflict with the above results (see Sec. 4).

We further assume that in the shattering case the available energy is partitioned in equal parts to the two colliding bodies (Hartmann, 1988), so for each of them fragmentation occurs if

$E_{rel} > 2SM/\rho x_{cr}$ (here x_{cr} is a numerical coefficient which will be justified later). The value of S is obtained from that observed in laboratory impact fragmentation experiments (S_0) through the scaling formula:

$$S_i = \left(S_{0,i} + \frac{\pi\gamma}{15} G \rho_i^2 D_i^2 \right) \left(\frac{D_i}{0.2\ m} \right)^{-1/4} , \tag{1}$$

where the term proportional to D^2 is due to self-compressional strengthening of the interior of each body (see Davis *et al.*, 1985), while the $D^{-1/4}$ factor is consistent with strain–rate scaling with size (Housen and Holsapple, 1990). The numerical coefficient γ is possibly material–dependent and has to be determined by experiments (see e.g. Housen *et al.*, 1991). For solid materials like basalt or concrete, abundant experimental evidence indicates that $S_0 \approx 3 \times 10^6\ J/m^3$.

Given S_i and the other impact parameters, our goal is to compute the mass distribution of the bodies generated by the impact. Since (i) this is is possible only for a finite number of target–projectile pairs (M_1, M_2), and (ii) it is normally useless to keep track of all the masses of the individual fragments, in our numerical computations we normally grouped the fragments into a limited number (ranging between ≈ 20 and 100) of discrete, logarithmic mass bins, having their limits (and central values) scaled by a constant amount (typically, a factor $g = 2$). In other words, we considered a geometric sequence of N_{bin} "central" mass values $m_{bin,k} = g^{k-1} m_{bin,1}$ $(k = 1, ..., N_{bin})$, with every bin spanning the range $(m_{bin,k}/\sqrt{g}, m_{bin,k}\sqrt{g})$. In order to compute the amount of mass reaccumulated by self–gravity after an impact, we also considered the fate of the low–mass "tail" of the distribution, ranging between the assumed lower cutoff of the fragment mass (M_{dust}, see later) and the lower limit of the first bin $(m_{bin,1}/\sqrt{g})$.

3 Shattering events

When one body is shattered, the mass of the largest remaining fragment is given by $M_{max,i} = M_i f_{l,i}$, where

$$f_{l,i} = \frac{1}{2} \left(\frac{S_i M_i}{\rho_i E_{rel}/2} \right)^{1.24} , \tag{2}$$

in agreement with the experimental relationship derived by Fujiwara *et al.* (1977), which predicts that when the critical energy threshold for fragmentation is just reached, a "core" half the mass of the original body survives, while this fraction decreases rapidly for increasing impact energies. Actually, the previous formula is valid for head–on impacts; if we take into account that oblique impacts are on the average less effective in shattering the involved bodies, $f_{l,i}$ can be averaged over the incidence angles leading to

$$\overline{f_{l,i}} = 3 f_{l,i}^{2/3} - 2 f_{l,i} \tag{3}$$

(Davis *et al.*, 1985). Hereinafter by $f_{l,i}$ we will always mean the averaged value $\overline{f_{l,i}}$ given by Eq.(3). In order to keep the definition of threshold collision as that generating a largest fragment with half the mass of the target, the condition for fragmentation given in Sec. 2 includes a numerical factor $x_{cr} = 4^{-1/1.24} \cong 0.327$, derived by noting that $\overline{f_{l,i}} = 1/2$ when $f_{l,i} = 1/8$. This implies that the effective strength of the targets versus impacts from random directions is about 3 times higher than the value found in the laboratory for head–on impacts.

Next, we need to model the mass distribution of the fragments. Following many previous investigations (e.g., Hartmann, 1969; Kresàk, 1977; Greenberg *et al.*, 1978; Zappalà *et al.*, 1984; Fujiwara *et al.*, 1989), we shall assume here a simple, albeit somewhat artificial, mathematical model: a *Pareto* power–law distribution truncated at a mimimum cut–off mass M_{dust} and consistent with the fact that $M_{max,i} = f_{l,i} M_i$ is the mass of the largest fragment. More precisely, we define $N_i(\geq m)$ to be the number of fragments of body i having mass larger than m and $M_i(\leq m)$ and $M_i(> m)$ the total mass of fragments of body i with an individual mass respectively smaller and larger than m; we assume that $N_i(\geq m)$ has a discontinuity at $m = M_{max,i}$ and that we know that there is just one fragment of mass $M_{max,i}$. If $\Theta(x)$ is the Heaviside step function ($= 0$ for $x < 0$ and $= 1$ for $x \geq 0$) and $\delta(x)$ is the Dirac delta function ($\delta(x) = d\Theta(x)/dx$), then we have

$$N_i(\geq m) = B_i m^{-b_i} \Theta(M_{max,i} - m) \Theta(m - M_{dust}) + B_i (M_{dust})^{-b_i} [1 - \Theta(m - M_{dust})] \ , \tag{4}$$

where b_i is the characteristic exponent of the cumulative size distribution, and $B_i = (M_{max,i})^{b_i}$, so that $N_i(\geq M_{max,i}) = 1$. The differential (or incremental) fragment size distribution is then given by:

$$\begin{aligned} n_i(m)\ dm &= -dN_i(\geq m) \\ &= \Big[b_i B_i m^{-b_i - 1} \Theta(M_{max,i} - m) + \delta(m - M_{max,i}) \Big] \Theta(m - M_{dust}) dm \ , \end{aligned} \tag{5}$$

while for the total mass accounted by fragments of mass smaller than any given value m we obtain (provided $b_i \neq 1$):

$$
\begin{aligned}
M_i(\leq m) &= \int_0^m m\ n_i(m)\ dm \\
&= \frac{b_i B_i}{1-b_i}\left[m^{1-b_i} - (M_{dust})^{1-b_i}\right]\left[1-\Theta(m-M_{max,i})\right] \\
&\quad + \left[\frac{b_i B_i}{1-b_i}\left[(M_{max,i})^{1-b_i} - (M_{dust})^{1-b_i}\right] + M_{max,i}\right]\Theta(m-M_{max,i})\ .
\end{aligned} \tag{6}
$$

Of course, the cumulative mass accounted by fragments larger than m will be $M_i(> m) = M_i - M_i(\leq m)$. Since mass conservation implies $M_i(\leq M_{max,i}) = M_i$, from Eq. (6) we get the condition

$$
M_i(1-f_{l,i}) = \frac{b_i B_i}{1-b_i}[(M_{max,i})^{1-b_i} - (M_{dust})^{1-b_i}]\ , \tag{7}
$$

which allows us to rewrite Eq.(6) as

$$
\begin{aligned}
M_i(\leq m) &= \frac{b_i (M_{max,i})^{b_i}}{1-b_i}\left[m^{1-b_i} - (M_{dust})^{1-b_i}\right]\left[1-\Theta(m-M_{max,i})\right] \\
&\quad + M_i\Theta(m-M_{max,i})\ .
\end{aligned} \tag{8}
$$

Eq.(7) is important because from it, once M_i, M_{dust} (which are "input parameters") and $f_{l,i}$ (or $M_{max,i}$, to be derived from Eqs.(2,3)) are known, the exponent b can be derived in a unique way. For this purpose, Eq.(7) can be rewritten as

$$
b = \frac{\frac{M}{M_{dust}}(1-f_l)}{\frac{M}{M_{dust}} - \left(\frac{M_{max}}{M_{dust}}\right)^b} \tag{9}
$$

and solved numerically by an iterative method. As pointed out with simplified formulae (ignoring e.g. the lower cutoff M_{dust}) by Greenberg *et al.* (1978) and Farinella *et al.* (1982), the assumption that the fragment mass distribution is given by a single–exponent power law allows us to uniquely specify its "free parameters" B_i and b_i. However, we have to stress here that this assumption is certainly an oversimplification of reality. Indeed, many experiments show that a much better fit is obtained by using different exponents in different mass ranges (Fujiwara *et al.*, 1989); the same property is shared by the real asteroid population (Cellino *et al.*, 1991). On the other hand, the physical meaning of the transition masses (or sizes) for which the best–fitting exponents change is not currently well understood; the corresponding values probably depend both on the material properties and on the impact parameters. As a consequence, we did not feel justified at this stage to introduce in our algorithm such a complicating feature as a two– or three–exponents power law to represent the fragment mass distribution — implying several more free parameters to be given in input, whose choice would be almost arbitrary.

It is easy to see that the critical value $b_i = 1$ separates the case in which most of the mass is in the largest bodies ($b_i < 1$) from the opposite one. Actually, note that when $M_{dust} \Rightarrow 0$, $b_i \Rightarrow 1 - f_{l,i}$ (rather than the commonly used relationship $b = (1 + f_l)^{-1}$, see e.g. Greenberg *et al.*, 1978). For $M_{dust} > 0$, the "supercatastrophic" cases when $f_l \ll 1$ can yield $b > 1$.

How many fragments are going to escape from the gravitational well of the two colliding bodies? A detailed answer would require the knowledge of the original position of the fragments inside their parent bodies, and of their motion immediately after the ejection. Although this problem could be tackled with models such as that of Paolicchi *et al.* (1989), its treatment is well beyond the scopes of the present work. Instead, we are going to derive an "effective escape velocity" V_{esc} defined by analogy with the usual definition of surface escape velocity of a celestial body, and to assume that only the fragments ejected with speeds exceeding V_{esc} will escape "to infinity" (i.e., will achieve independent heliocentric orbits). We use the energy balance equation

$$\frac{1}{2}(M_1 - M_{max,1} + M_2 - M_{max,2})V_{esc}^2 + W_{tot} = W_{fr,1} + W_{fr,2} + W_h \ , \tag{10}$$

where we have assumed that after the impact both the colliding bodies are shattered (if this is not the case for body i, $W_{fr,i}$ will have to be changed into $W_{crat,i}$, to be derived in Sec. 4) and that the largest fragment from either of them has negligible kinetic energy (this is consistent with experimental results by Fujiwara and Tsukamoto, 1980, Nakamura and Fujiwara, 1991, and others). The various W terms in Eq.(10) stand for the following potential energies: W_{tot} is the total potential energy of the two bodies just before fragmentation, that is

$$W_{tot} = -\frac{3GM_1^{5/3}}{5Q_1} - \frac{3GM_2^{5/3}}{5Q_2} - \frac{GM_1M_2}{Q_1M_1^{1/3} + Q_2M_2^{1/3}} \ , \tag{11}$$

where $Q_i = (4\pi\rho_i/3)^{-1/3}$; $W_{fr,i}$ is the sum of the self-gravitation potential energy of each fragment of body i, derived form the mass distribution (5):

$$W_{fr,i} = \frac{3G}{5Q_i}\int_{m=0}^{m=\infty} m^{5/3} \ n_i(m) \ dm = -\frac{3G}{5Q_i}\frac{5M_{max,i}^{5/3} - 3b_iM_{max,i}^{b_i}M_{dust}^{5/3-b_i}}{5 - 3b_i} \tag{12}$$

and W_h is an estimate of the potential energy when the escaped fragments are separated by a distance of the order of the Hill's radius of the total colliding mass in the gravitational field of the central mass (for the asteroids, the Sun) of mass M_0 and orbital distance R_0:

$$W_h = -\frac{3G(M_1+M_2)^{5/3}}{5}\frac{(3M_0)^{1/3}}{R_0} \ . \tag{13}$$

4 Cratering events

Assume now that for body i, $E_{rel} < 2S_iM_i/\rho_i x_{cr}$, so that it is not shattered by the collision. In this case a crater is formed on it. If the case of a small–scale collision, resulting into a crater of mass smaller than 1% of the target mass, we assume that the mass M_{crat} excavated from the crater (and converted into ejected fragments) is just proportional to the impact energy, through a *crater excavation coefficient* α to be given in input and depending on the material properties (for "soft" and "hard" materials, laboratory data yield $\alpha \approx 4 \times 10^{-4}\ s^2/m^2$ and $\alpha \approx 10^{-5}\ s^2/m^2$, respectively; see Stöffler *et al.*, 1975, and Dobrovolskis and Burns, 1984, p. 467). For larger craters, we still assume a linear dependence of the excavated mass on E_{rel}, but with coefficients such that the largest possible crater — created when E_{rel} is just less than the fragmentation threshold $2S_iM_i/\rho_i x_{cr}$ — has a mass of 1/10 that of the target. Note that this is much more than the largest crater predicted by conventional scaling theories, which has a diameter of the order of the target radius and a volume $\approx 3\%$ of the target volume; rather, our assumption is in agreement with the recent results of numerical hydrocode simulations of asteroid impacts, suggesting that such giant craters (or concavities) can be formed without complete break–up of the target, but damaging the material structure enough for generating a substantial amount of regolith (Greenberg *et al.*, 1992).

Imposing continuity for $M_{crat} = M_i/100$, we obtain the relationships

$$M_{crat} = \alpha E_{rel} \qquad \text{for} \quad E_{rel} \leq \frac{M_i}{100\alpha} \ , \tag{14}$$

$$M_{crat} = \frac{9\rho_i x_{cr}\alpha}{200S_i\alpha - \rho_i x_{cr}}E_{rel} + \frac{M_i}{10}\frac{\rho_i x_{cr} - 20S_i\alpha}{\rho_i x_{cr} - 200S_i\alpha} \qquad \text{for} \quad \frac{M_i}{100\alpha} < E_{rel} \ , \tag{15}$$

In the cratering case, the largest surviving body has always a mass $M_i - M_{crat}$; we shall again assume a single–exponent power law mass distribution of the ejected fragments, but with an exponent b_i having the constant value 0.8, instead of being related to the impact parameters (as in the shattering case). As a consequence, the largest fragment from the crater has a mass $f_{l,i}M_{crat}$, with $f_{l,i}$ given by the implicit equation

$$f_{l,i} = 1 - b_i + b_i f_{l,i}^{b_i}\left(\frac{M_{dust}}{M_{crat}}\right)^{1-b_i} \ , \tag{16}$$

which can be easily solved numerically. Also, in the cratering case the post–impact potential energy is given by

$$\begin{aligned} W_{crat,1} &= -\frac{3G}{5Q_i}\int_{m=0}^{m=\infty} m^{5/3}\ n_i(m)\ dm - \frac{3G(M_i - M_{crat})^{5/3}}{5Q_i} \\ &= -\frac{3G}{5Q_i}\frac{5M_{max,i}^{5/3} - 3b_i M_{max,i}^{b_i} M_{dust}^{5/3-b_i}}{5-3b_i} - \frac{3G(M_i - M_{crat})^{5/3}}{5Q_i}\ , \end{aligned} \tag{17}$$

which has to be substituted in Eq.(10) for V_{esc} instead of $W_{fr,i}$.

5 Ejection velocity vs. mass relationship and reaccumulation

Most models of asteroid collisional evolution (e.g., Davis *et al.*, 1985, 1989) neglect any possible correlation between the ejection velocity and the mass of the fragments (both from shattering and for cratering events), and just assume that the fraction of the total fragment mass ejected with speeds exceeding some given value V is $(V/V_{min})^{-k}$, V_{min} being a fixed lower cutoff to the ejection velocity. Such a relationship was observed for crater ejecta (with $k \approx 9/4$) by Gault *et al.* (1963), and later confirmed by other experiments. On the other hand, recent experimental evidence (Davis and Ryan, 1990; Nakamura and Fujiwara, 1991) indicates that some correlation exists, with the largest fragments normally going somewhat slower; this is also predicted by the semiempirical models of Paolicchi *et al.*, 1989, 1992). It is easy to show (see e.g. Nakamura and Fujiwara, 1991) that in this case the relationship given above for the mass fraction ejected at speeds $> V$ still holds provided the fragment speeds are proportional to the power $-r$ of their mass, with $r = (1-b)/k$.

Here we shall assume that there is a definite correlation between the mass and the velocity of a fragment, which is modelled either in a deterministic way (e.g., through a definite formula relating the two quantities), or stochastically (see later). We define $E_i = E_{rel}/2$ as the energy received by body i at impact, and $E_{fr,i} = f_{ke}E_i$ as the total kinetic energy of ejecta from body i, where f_{ke} is an input parameter specifying which fraction of the impact energy is partitioned into kinetic energy of the fragments (for a detailed discussion about this *anelasticity parameter*, see Davis *et al.*, 1989). In order to avoid any possible divergence of the kinetic energy of the fragments, we set a high velocity cutoff V_{max} to the distribution (a reasonable phyical motivation for this is that the fragment velocity is unlikely to exceed the sound velocity in the material, of the order of some km/s). To give the explicit relationship between the velocity v and the mass m of a fragment, we must distinguish two cases according to the sign of r_i. If $r_i > 0$:

$$\begin{aligned} v &= C_i m^{-r_i} && \text{for} \quad \bar{M_i} \leq m \leq M_{max,i} \\ v &= V_{max} && \text{for} \quad m < \bar{M_i} \ . \end{aligned} \tag{18}$$

where $\bar{M_i} = (V_{max}/C_i)^{-1/r_i}$. On the other hand, if $r_i < 0$ (this case is treated for consistency, see later):

$$\begin{aligned} v &= C_i m^{-r_i} && \text{for} \quad M_{dust} \leq m \leq \bar{M_i} \\ v &= V_{max} && \text{for} \quad \bar{M_i} < m \ . \end{aligned} \tag{19}$$

The constant coefficient C_i is obtained from an energy conservation equation. Consistently with the definition of V_{esc}, in the shattering case the largest fragment is assumed to have a negligible kinetic energy in the reference frame of the center of mass. On the other hand, this is not true in the cratering case. Therefore, we will insert the corresponding term in the conservation equation multiplied by a factor λ_i, with $\lambda_i = 0$ for shattering and $\lambda_i = 1$ for cratering. We also define $\bar{V_i} = C_i \left(M_{max,i}\right)^{-r_i}$. We now have two possibilities: either for all fragments $C_i m^{-r_i}$ is smaller than V_{max}, in which case we just solve the equation:

$$\begin{aligned} E_{fr,i} &= \lim_{\epsilon \to 0} \int_{M_{dust}}^{M_{max,i}-\epsilon} \frac{v^2}{2} m n_i(m) dm + \lambda_i \frac{\bar{V}_i^2}{2} M_{max,i} \\ &= \lambda_i C_i^2 \frac{M_{max,i}^{1-2r_i}}{2} + \frac{C_i^2}{2} \frac{b_i M_{max,i}^{b_i}}{1-b_i-2r_i} \left[M_{max,i}^{1-b_i-2r_i} - M_{dust}^{1-b_i-2r_i} \right] \end{aligned} \tag{20}$$

and obtain

$$C_i = \sqrt{\frac{2E_{fr,i}}{\lambda_i M_{max,i}^{1-2r_i} + \frac{b_i M_{max,i}^{b_i}}{1-b_i-2r_i} \left[M_{max,i}^{1-b_i-2r_i} - M_{dust}^{1-b_i-2r_i} \right]}} \ , \tag{21}$$

or for some fragments (i.e. those having mass M_{dust} if $r_i > 0$ or $M_{max,i}$ if $r_i < 0$) $C_i m^{-r_i} > V_{max}$, in which case the correct equations are different depending on the sign of r_i: for $r_i > 0$ we have

$$E_{fr,i} = \lim_{\epsilon \to 0} \int_{\bar{M}_i}^{M_{max,i}-\epsilon} \frac{v^2}{2} m n_i(m) dm + \frac{V_{max}^2}{2} M(\leq \bar{M}_i) + \lambda_i \frac{\bar{V}_i^2}{2} M_{max,i} \ , \tag{22}$$

$$M(\leq \bar{M}_i) = \frac{b_i}{1-b_i} M_{max,i}^{b_i} \left[\bar{M}_i^{1-b_i} - M_{dust}^{1-b_i} \right] \tag{23}$$

and

$$\begin{aligned} E_{fr,i} &= \lambda_i C_i^2 \frac{M_{max,i}^{1-2r_i}}{2} + \frac{V_{max}^2}{2} \frac{b_i}{1-b_i} M_{max,i}^{b_i} \left[\bar{M}_i^{1-b_i} - M_{dust}^{1-b_i} \right] \\ &\quad + \frac{C_i^2}{2} \frac{b_i M_{max,i}^{b_i}}{1-b_i-2r_i} \left[M_{max,i}^{1-b_i-2r_i} - \bar{M}_i^{1-b_i-2r_i} \right] \\ &= C_i^2 \frac{M_{max,i}^{1-2r_i}}{2} \left[\lambda_i + \frac{b_i}{1-b_i-2r_i} \right] + C_i^{k_i} b_i \frac{M_{max,i}^{b_i} V_{max}^{2-k_i}}{2} \left[\frac{1}{1-b_i} - \frac{1}{1-b_i-2r_i} \right] \\ &\quad - \frac{V_{max}^2}{2} \frac{b_i}{1-b_i} M_{max,i}^{b_i} M_{dust}^{1-b_i} \ ; \end{aligned} \tag{24}$$

on the other hand, for $r_i < 0$ we have:

$$E_{fr,i} = \int_{M_{dust}}^{\bar{M}_i} \frac{v^2}{2} m n_i(m) dm + \frac{V_{max}^2}{2} M(> \bar{M}_i) \ , \tag{25}$$

$$M(> \bar{M}_i) = \frac{b_i}{1-b_i} M_{max,i}^{b_i} \left[M_{max,i}^{1-b_i} - \bar{M}_i^{1-b_i} \right] + \lambda_i M_{max,i} \ , \tag{26}$$

$$\begin{aligned} E_{fr,i} &= \frac{V_{max}^2}{2} \frac{b_i M_{max,i}^{b_i}}{1-b_i} \left[M_{max,i}^{1-b_i} - \bar{M}_i^{1-b_i} \right] + \lambda_i \frac{V_{max}^2}{2} M_{max,i} \\ &\quad + \frac{C_i^2}{2} \frac{b_i M_{max,i}^{b_i}}{1-b_i-2r_i} \left[\bar{M}_i^{1-b_i-2r_i} - M_{dust}^{1-b_i-2r_i} \right] \\ &= -C_i^2 \frac{M_{max,i}^{b_i}}{2} \frac{b_i}{1-b_i-2r_i} M_{dust}^{1-b_i-2r_i} + C_i^{k_i} b_i \frac{M_{max,i}^{b_i} V_{max}^{2-k_i}}{2} \left[\frac{1}{1-b_i-2r_i} - \frac{1}{1-b_i} \right] \\ &\quad + \frac{V_{max}^2}{2} M_{max,i} \left[\lambda_i + \frac{b_i}{1-b_i} \right] \ . \end{aligned} \tag{27}$$

Thus, C_i is the solution of the equation

$$a C_i^{k_i} + b - C_i^2 = 0 \ , \tag{28}$$

where

$$
\begin{aligned}
a &= M_{max,i}^{2r_i+b_i-1} V_{max}^{2-k_i} \left[\frac{2b_i r_i}{\left[(1-2r_i-b_i)\lambda_i + b_i\right](1-b_i)} \right] \\
b &= 2M_{max,i}^{2r_i-1} \left[\frac{1-b_i-2r_i}{(1-2r_i-b_i)\lambda_i + b_i} \right] \left[E_{fr,i} + \frac{V_{max}^2}{2} \frac{b_i}{1-b_i} M_{max,i}^{b_i} M_{dust}^{1-b_i} \right]
\end{aligned} \tag{29}
$$

for $r_i > 0$, and:

$$
\begin{aligned}
a &= M_{dust}^{2r_i+b_i-1} V_{max}^{2-k_i} \left[\frac{2r_i}{1-b_i} \right] \\
b &= 2M_{dust}^{2r_i+b_i-1} M_{max,i}^{-b_i} \left[\frac{b_i+2r_i-1}{b_i} \right] \left[E_{fr,i} - \frac{V_{max}^2}{2} M_{max,i} \left(\lambda_i + \frac{b_i}{1-b_i} \right) \right]
\end{aligned} \tag{30}
$$

for $r_i < 0$. Our program first tries the explicit formula (19); then, if the V_{max} cutoff turns out to be relevant, it solves numerically Eqs. (22). Also, we keep the freedom of giving as an input parameter either r_i or k_i, and then deriving the other one through the simple relationship

$$
r_i = \frac{1-b_i}{k_i} \; . \tag{31}
$$

This implies that in the “supercatastrophic” case $b_i > 1$, when most of the fragment mass is concentrated at small sizes, we obtain the somewhat counterintuitive result that either r_i or k_i has a negative value.

All the previous formulae have been derived for a *deterministic* relationship between v and m, as given by Eqs. (17). A more realistic treatment may assume that the same relationship has instead a probabilistic nature, i.e., it holds for the r.m.s. value $V_0 = \sqrt{\langle v^2 \rangle}$ of a Maxwellian distribution function for v:

$$
P(v; V_0) = \sqrt{\frac{2}{\pi}} \, \frac{3\sqrt{3}v^2}{V_0^3} \, \exp\left(-\frac{3v^2}{2V_0^2} \right) \; . \tag{32}
$$

Note that the mean kinetic energy for bodies of a given mass m is still given by $mV_0^2/2$. Therefore, neglecting statistical fluctuations, we can keep the same energy conservation equations obtained before to compute the constant C_i in this case (provided V_{max} is now interpreted as the higher cutoff to V_0). Also in this *probabilistic* case, we have the choice of fixing in input either r_i or k_i.

The self–gravitational reaccumulation process is then treated as follows. The impact is assumed to always generate a remnant body formed by the two largest remnants from the colliding bodies (either the largest shattered fragment(s) or the cratered target(s)), plus the non–escaping fraction of the smaller fragments. Let us define $M_{esc,i} = (C_i/V_{esc})^{1/r_i}$, namely the mass corresponding to the escape velocity. In the deterministic case, if $r_i > 0$, the reaccumulated (non–escaping) fragments are those with mass in the range between $\max(M_{dust}, M_{esc,i})$ and $M_{max,i}$; if $r_i < 0$, the reaccumulation range is between M_{dust} and $\min(M_{esc,i}, M_{max,i})$. The corresponding total mass is easily found by integrating between these limits $m.n_i(m)dm$, with $n_i(m)dm$ given by Eq.(5).

In the probabilistic case, the whole range between M_{dust} and $M_{max,i}$ is considered. For the mass bins containing ≤ 100 bodies, the non–escaping fragments are drawn at random by using the velocity distribution (24) — more precisely, given V_0 (derived from m through equations similar to (17)), a number is drawn at random according to the distribution (24), and then compared to V_{esc}. For the mass bins containing more than 100 fragments, we just compute the fraction of non–escaping fragments f from

$$f = \int_0^{V_{esc}} \sqrt{\frac{2}{\pi}} \frac{3\sqrt{3}v^2}{V_0^3} \exp -\frac{3v^2}{2V_0^2} dv \; ; \tag{33}$$

calling $\mathrm{erf}(v)$ the error function

$$\mathrm{erf}(v) = \frac{2}{\sqrt{\pi}} \int_0^v \exp -x^2 dx \; , \tag{34}$$

we get

$$f = -\frac{2}{\sqrt{\pi}} \sqrt{\frac{3}{2}} \frac{V_{esc}}{V_0} \exp -\frac{3V_{esc}^2}{2V_0^2} + \mathrm{erf}\left(\sqrt{\frac{3}{2}} \frac{V_{esc}}{V_0}\right) \; . \tag{35}$$

As for the "tail" of the mass distribution (i.e., the fragments having masses between M_{dust} and the lower limit of the smallest mass bin, $m_{bin,1}/\sqrt{g}$), we keep the option of dealing with it "deterministically" or in agreement with the probabilistic procedure. In the former case, the reaccumulated tail mass is the integral of $m.n_i(m)dm$ between the values $\max(M_{dust}, M_{esc,i})$ and $\min(M_{max,i}, m_{bin,1}/\sqrt{g})$ (provided $r_i > 0$), or between M_{dust} and $\min(M_{esc,i}, M_{max,i}, m_{bin,1}/\sqrt{g})$ (if $r_i < 0$).

On the other hand, the "probabilistic" tail treatment is done by taking into account the velocity distribution (24). This is made by evaluating the double integral

$$I = bM_{max}^b \int_{M_{dust}}^{m_{bin,1}/\sqrt{g}} \int_0^{V_{esc}} P(v; V_0(m)) m^{-b} dv \, dm \; . \tag{36}$$

If $V_0 = V_{max}$, the integral over the mass can be done analytically and that over the velocity reduces to (25); otherwise a numerical calculation is carried out.

6 Some results and applications

In this Section we shall illustrate some results of our model by means of appropriate plots. We are not going here to explore systematically the multi–dimensional space of our input model parameters in order to study how the collision outcomes depend on them, but only to touch on some specific issues, which we believe are important from the physical point of view. Therefore, we have assumed a set of *nominal* input values as follows: density $\rho = 2500\ kg/m^3$; impact velocity $V_{rel} = 5.81\ km/s$; lower cutoff of the fragment mass $M_{dust} = 10^{-5}\ kg$; higher cutoff of the fragment ejection velocity $V_{max} = 5\ km/s$; pre–scaling impact strength $S_0 = 3 \times 10^6\ J/m^3$ (S was then derived by means of Eq. (1), with $\gamma = 1$); anelasticity parameter $f_{ke} = 0.1$; crater excavation coefficient $\alpha = 10^{-4}\ s^2/m^2$. For our numerical computations we used 50 logarithmic mass bins spaced by a factor 2 (i.e., a factor 1.26 in size), with central values of the corresponding radii ranging from $1.211 \times 10^{-2}\,km$ to $10^3\,km$.

Figs. 1 and 2 give an idea of the mass distribution predicted by the model for shattered bodies of radii ranging from $1\,km$ to $10^3\,km$ (roughly, the size range where most observable asteroids and natural satellites are found). We have plotted in the same frame the mass ratio f_l between the largest fragment and the target (or the total mass excavated in the crater) and the exponent b of the cumulative fragment mass distribution (see Eqs. (2), (3) and (9)) versus the logarithm of the radius R of the parent body, by taking a fixed value (either 10^{-4} or 10^{-3}) of the projectile–to–target mass ratio M_2/M_1. As shown by Fig. 1, both b and f_l approach the limit value 1/2 when M_2/M_1 and R are such that the threshold between shattering and cratering impacts is reached (this occurs going towards larger target radii, due to the increase of S with size (see Eq.(1)). b is of course closer to 1 (and f_l to zero) for more disruptive collisions, owing to a lower strength or a larger projectile–to–target mass ratio. For craters, on the other hand, both b and f_l are assumed to have constant values (see Sec. 4). Notice that for the nominal values of S_0 and V_{rel}, a collision involving a projectile of 1/10 the size of the target normally causes extensive break–up, and generates a swarm of fairly small fragments. For an asteroid $200\,km$ across, such as the parent bodies of several asteroid families, the average collision rate quoted in Sec. 1 implies that such collisions have a probability of order unity of occurring over the solar system lifetime (taking into account that several thousands of bodies of diameter $\approx 20\,km$ exist in the main asteroid belt, see Cellino *et al.*, 1991).

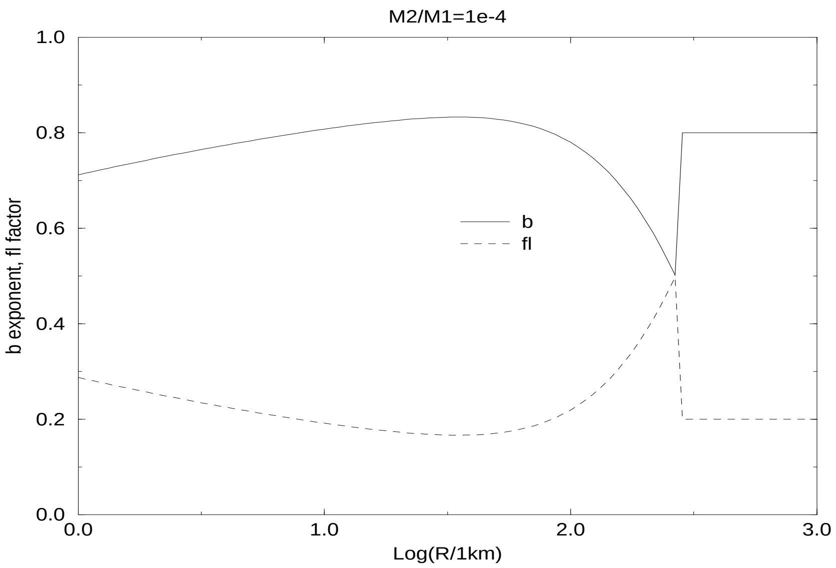

Fig. 1: b and f_l versus the logarithm of the radius of the parent body for the nominal values of the impact parameters and a projectile–to–target mass ratio of 10^{-4}.

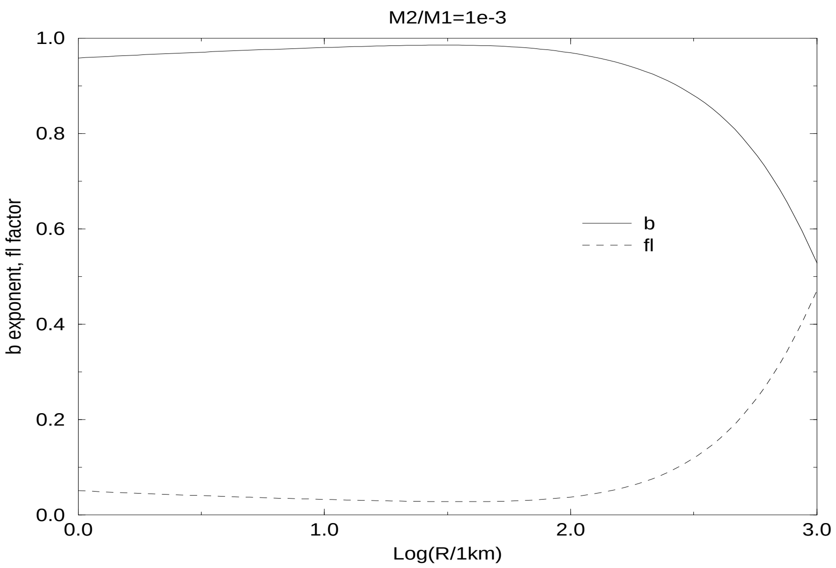

Fig. 2: The same as Fig. 1, but for $M_2/M_1 = 10^{-3}$.

The curves shown in Figs. 1 and 2 are not significantly changed when the lower mass cutoff of the fragments M_{dust} is modified within reasonable bounds. Actually, as discussed in Sec. 3, this parameter becomes relevant only for *supercatastrophic* impacts, namely when b is close to 1. This is illustrated in Fig. 3, where the relationship between f_l and b is plotted for three values of M_{dust} (differing from each other by orders of magnitude) in the supercatastrophic case $M_2/M_1 = 1$. Note that for b smaller than unity the approximation $f_l \cong (1-b)$, which corresponds to the limit $M_{dust} \Rightarrow 0$, is fairly accurate.

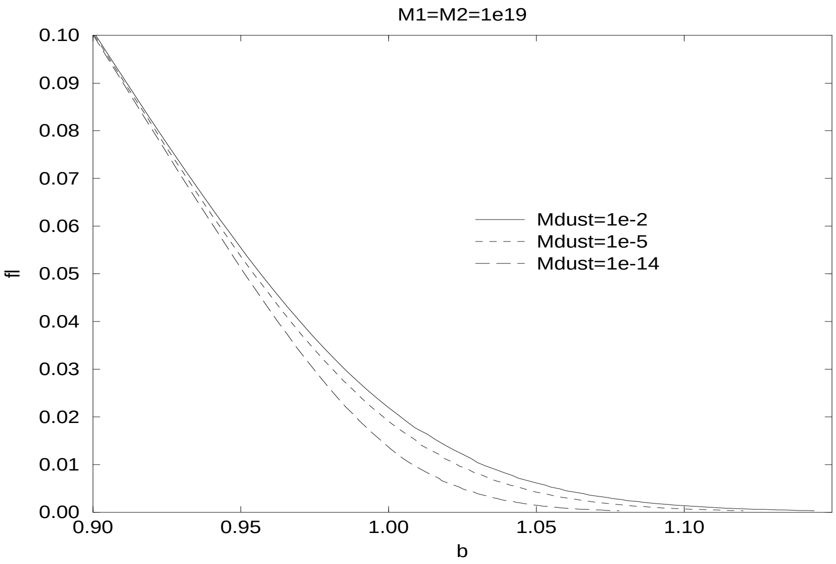

Fig. 3: f_l versus b for $M_1 = M_2 = 10^{19}$ kg and different values of M_{dust}.

Fig. 4 shows, for three different values of the projectile–to–target mass ratio, how the averaged escape velocity V_{esc} defined by Eq.(10) (normalized to the surface escape velocity of M_1) varies as a function of b. As shown by Farinella *et al.* (1988), when $M_2 \ll M_1$ and b is close to 1, the limiting value of the normalized escape velocity is about 0.77. The curves shown in Fig. 4 are somewhat different from that appearing in Fig. 1 of the above–mentioned paper, because (i) we now take into account the mass of the projectile (so the curves are shifted upward for higher values of M_2/M_1), and (ii) we have made the assumption that the largest fragment, whose mass is higher for smaller values of b, has always a negligible kinetic energy. Fig. 4 shows that taking a constant value ≈ 0.8 for the normalized escape velocity after shattering impacts is normally a good approximation. As shown by Fig. 5, using $M_{dust} > 0$ has little influence on the escape velocity.

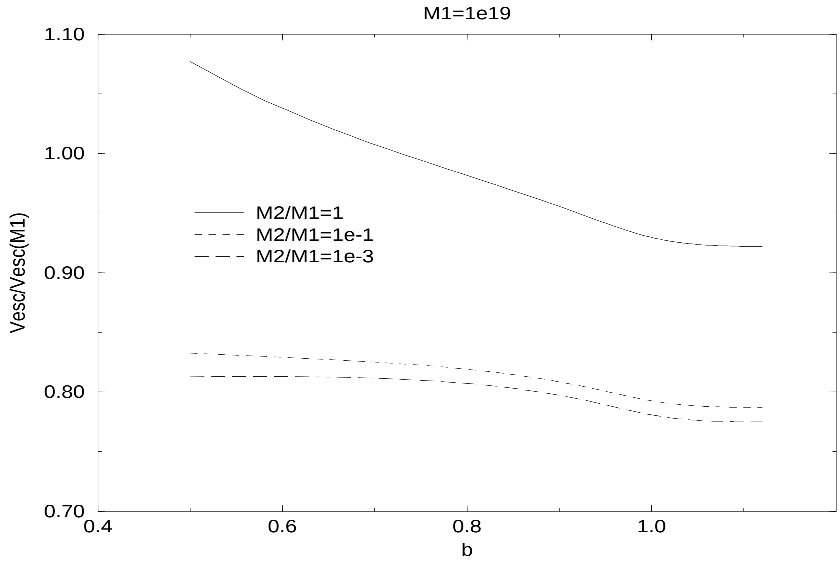

Fig. 4: The average fragment escape velocity, normalized to the surface escape velocity of M_1, versus b for three different values of the projectile–to–target mass ratio.

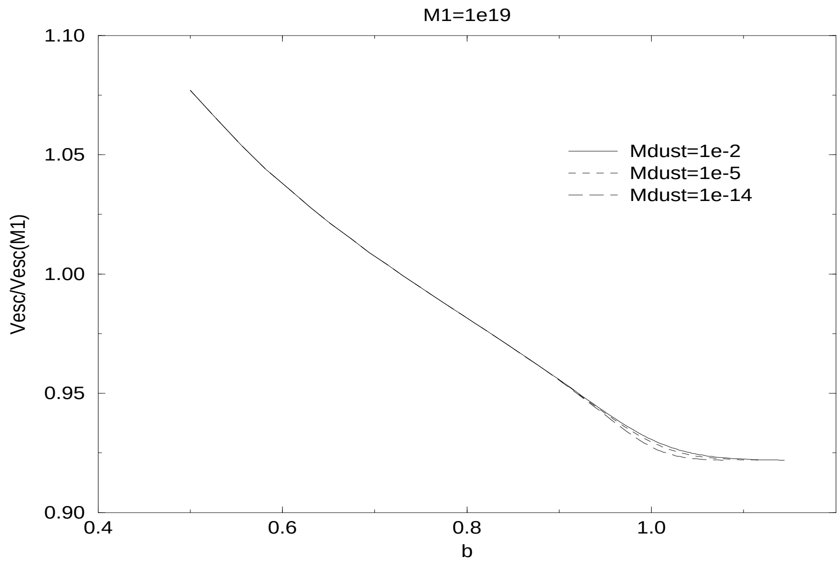

Fig. 5: The same as Fig. 4 for $M_2/M_1 = 1$, but for three different values of M_{dust}.

One of the most interesting aspects of the algorithm presented in this paper is that it allows us to model in several alternative ways the gravitational reaccumulation process, through the use of different fragment velocity vs. mass relationships, as discussed in Sec. 5. Qualitatively speaking, the reaccumulation process is due to the fact that, for targets having escape velocities of tens to hundreds of m/s, the amount of energy sufficient for fragmenting them is normally not enough to accelerate all the fragments to speeds exceeding V_{esc}. Thus the slower fragments fall back and reaccumulate onto the largest one, giving rise to a so–called *pile of rubble*. The relevance of this process for asteroid evolution has been discussed in detail more than a decade ago by Davis *et al.* (1979) and Farinella *et al.* (1982). But of course the quantitative aspects of it depend in a critical manner on the conversion efficiency of the projectile's kinetic energy into kinetic energy of fragments (i.e., the *anelasticity coefficient* f_{ke}), as well as on the way the available kinetic energy is partitioned among fragments of different masses. We shall focus here on the latter issue.

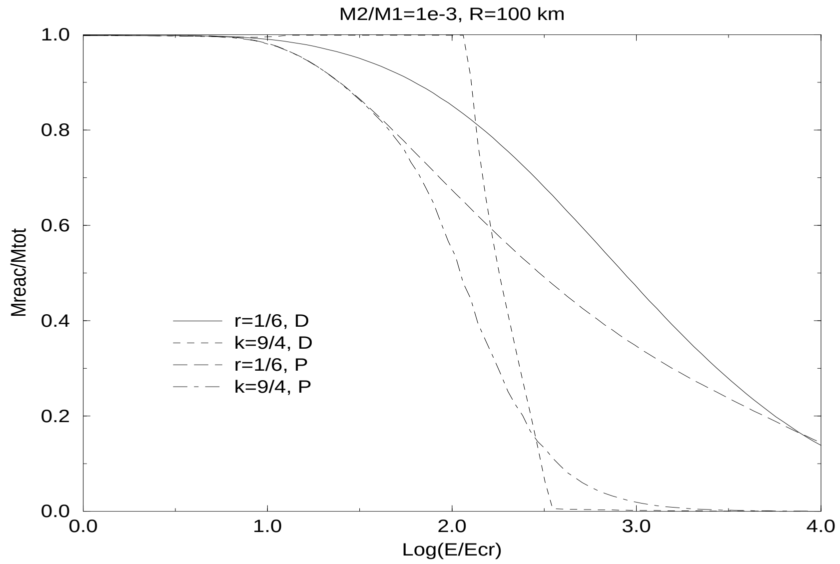

Figure 6. The fraction of reaccumulated mass for an impact with $M_2/M_1 = 10^{-3}$ against a target of radius $100\,km$, versus the logarithm of the impact energy. The latter parameter is normalized to the minimum energy required for fragmentation. Different fragment velocity vs. mass relationships are used (see text), with D standing for "deterministic model" and P for "probabilistic model".

Fig. 6 shows, for a target $100\,km$ in radius and $M_2/M_1 = 10^{-3}$, the fraction of reaccumulated mass versus the logarithm of the impact energy, normalized to the critical energy for fragmentation. Clearly, with our nominal parameter choice, there is a gap of more than two orders of magnitude between the fragmentation threshold and the energy needed to disperse to infinity a significant fraction of the target mass. As a consequence, most asteroids of radius $\approx 100\,km$ have been probably shattered but not *disrupted* (i.e., have reaccumulated) as a consequence of the most energetic collisions they have undergone over the history of the solar system. Fig. 6 also shows that the reaccumulation process is confined to a narrow energy range if we assume $k = 9/4$, i.e. we require that for every velocity V (exceeding a lower cutoff) the total mass ejected with higher speeds is $\propto V^{-9/4}$. The reason for this is that since $r = (1-b)/k$ (see Sec. 5) and b is close to 1 (see Fig. 2), the exponent r in this case is small, implying that the velocity of fragments has a weak dependence on their mass: thus, there is an abrupt transition between the case when nearly all the fragments are slower than V_{esc} and the opposite one. The transition is less sharp in the probabilistic case, since in this case for every mass the fragment velocities have a significant chance variability — and it is much smoother when r (instead of k) is fixed to the value 1/6, consistent with experimental data. In this case, even after a supercatastrophic impact a significant fraction of mass is always reaccumulated, because most of the mass resides in small fragments and is forced to move comparatively fast, so that

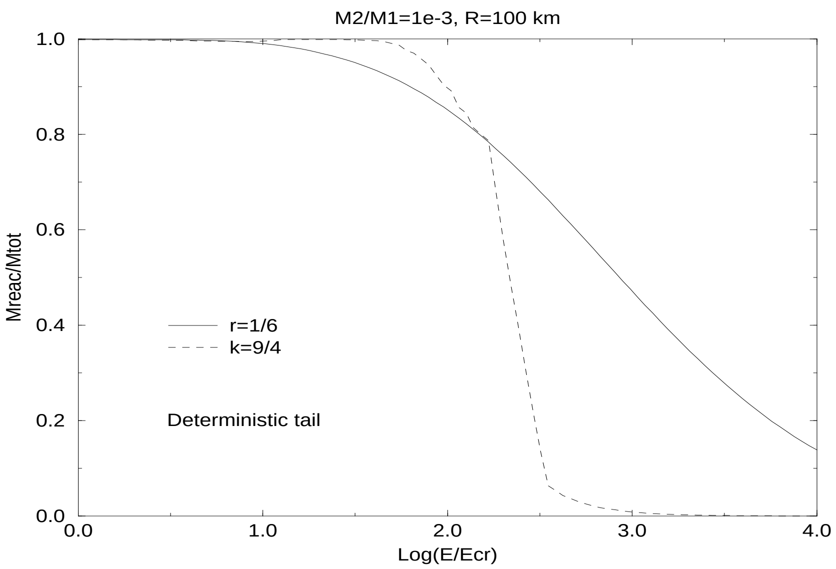

Figure 7. The same as Fig. 6, but treating always in a deterministic case the small–size tail of the fragment mass distribution.

conservation of energy causes the largest fragments to be slow and to reaccumulate. Fig. 7 shows what happens if the bodies in the small–size tail of the mass distribution (fragments smaller than about 20 m) are treated deterministically, as described in Sec. 5: while the

$r = 1/6$ curve is unaffected, because in this case the tail fragments are always fast enough to escape, there is a significant change in the $k = 9/4$ case.

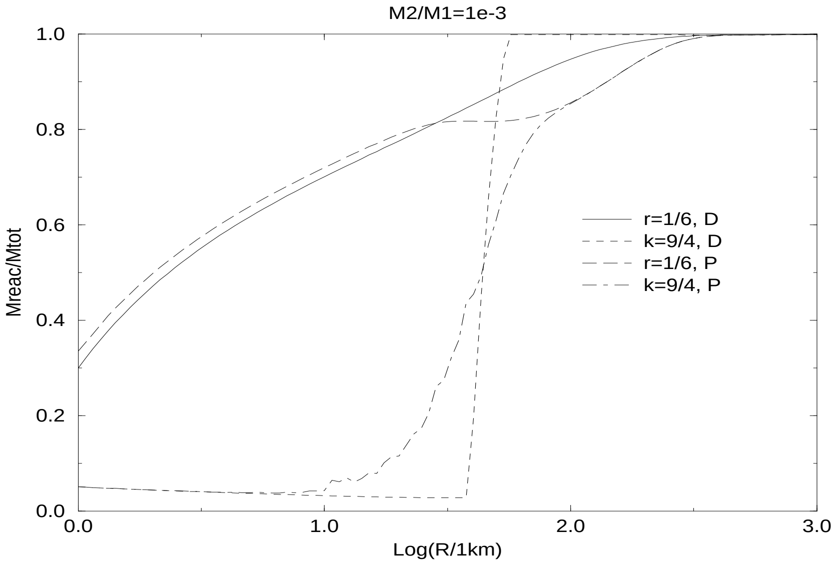

Fig. 8: The fraction of reaccumulated mass for a shattering impact with $M_2/M_1 = 10^{-3}$ versus the logarithm of the target radius. The same four models have been used as in Fig. 6.

A physically important consequence of the different behaviors of the $k = 9/4$ and the $r = 1/6$ models is apparent from Figs. 8 and 9, which give, for the same models used to draw Fig. 6 and 7, the fraction of reaccumulated mass versus target size. Again, for the $k = 9/4$ models (but less for the probabilistic ones), there is a comparatively sudden transition from negligible to substantial reaccumulation, which occurs when the velocity of most fragments becomes lower than V_{esc}. This would imply comparatively short collisional lifetimes of small asteroids — say, in the 1 to 50 km diameter range. Also, in this case small asteroids would be unlikely to be *rubble piles*, but would mostly look like single, competent fragments. The opposite conclusion would follow from the $r = 1/6$ models, for which the figures show that even small bodies are always reaccumulated; recall, however, that when V_{esc} is small only a small number of massive fragments may become reaggregated. This is possibly an effective mechanism to form km–sized contact or nearly–contact binary asteroids, such as recently observed by radar (Ostro *et al.*, 1990).

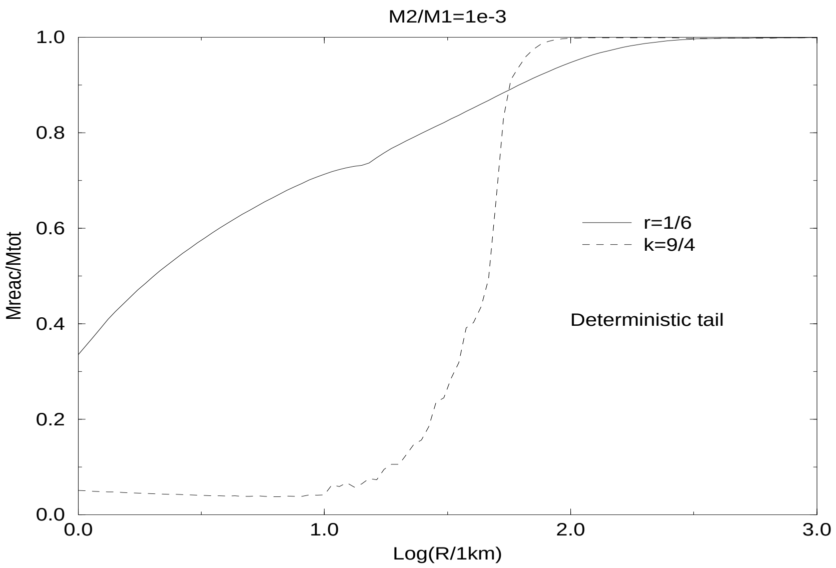

Fig. 9: The same as Fig. 8, but treating always in a deterministic case the small–size tail of the fragment mass distribution.

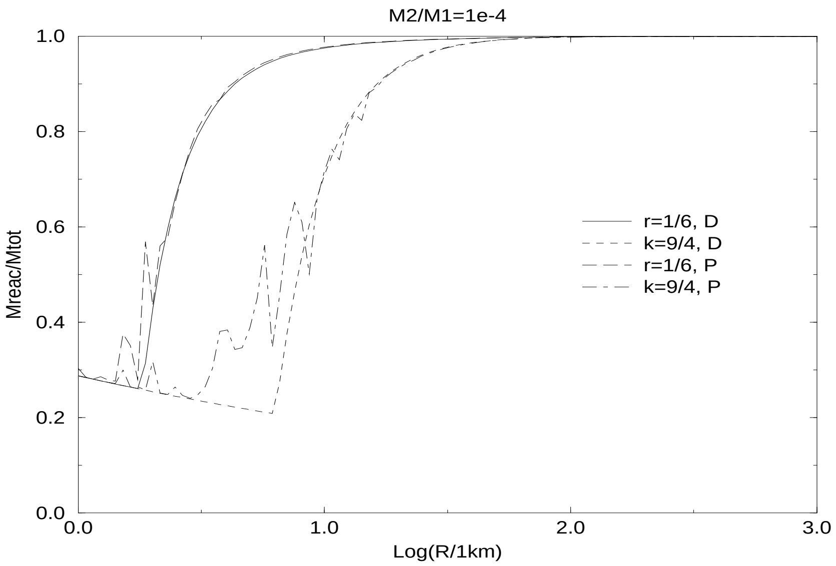

Fig. 10: The same as Fig. 8, but for $M_2/M_1 = 10^{-4}$.

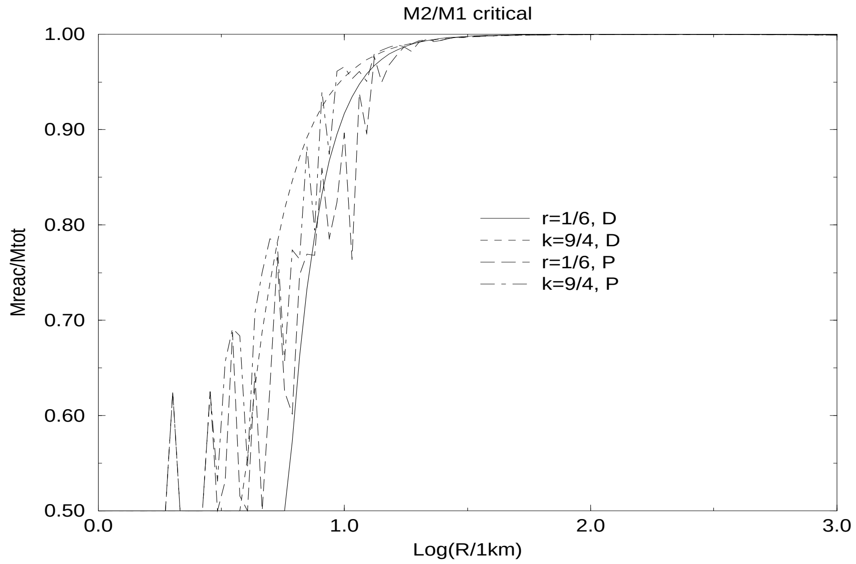

Fig. 11: The same as Fig. 8, but for M_2/M_1 just exceeding the threshold value for fragmentation.

For a smaller projectile–to–target mass ratio (10^{-4}, still sufficient for fragmentation), Fig. 10 shows that both the $r = 1/6$ models and the $k = 9/4$ models display a transition from complete fragment escape (with the chance exception of some large fragments in the probabilistic cases, giving rise to irregular curves) to substantial reaccumulation. Of course here the transition occurs at smaller target sizes (less than $10\,km$ radius), but there is a shift of about a factor 3 between the two types of models, due to the lower velocity of the big fragments in the $r = 1/6$ cases. For a barely shattering impact (Fig. 11), on the other hand, all the models yield similar results, with the transition occurring at a radius of $\approx 5\ km$ (plus or minus a factor 2) and large fluctuations in the probabilistic cases.

When $M_2/M_1 = 10^{-5}$, we are in the cratering case (see Sec. 4), with Eqs.(14) yielding between 2% and 3% of excavated mass (see Fig. 12; the crater mass increases with target size because of the decreasing impact strength in this size range). Again the reaccumulation of crater ejecta is effective at smaller sizes in the $r = 1/6$ models, and is anyway practically complete for bodies exceeding 100 km diameter.

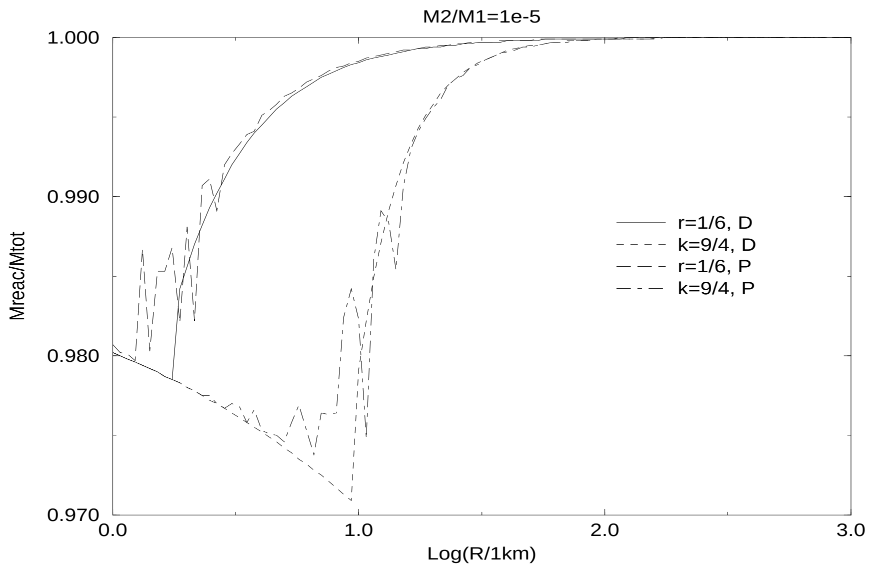

Fig. 12: The same as Fig. 8, but for $M_2/M_1 = 10^{-5}$. This mass ratio results in a cratering event.

These results provide some hints to the collisional history of 951 Gaspra, the asteroid about $13\,km$ in mean diameter recently approached and imaged by the Galileo probe (Belton *et al.*, 1992). Gaspra's global shape is strongly irregular, with two very large concavities (about $8\,km$ across) evident on its limb. However, the general appearance of the surface is fairly smooth, with no sharp edges and a relative paucity of km–sized craters (while several linear "grooves" are apparent). To explain these features and the distribution of colors and albedo variations, which hints to the presence of surface regolith, Greenberg *et al.* (1992) have suggested that Gaspra's interior is a rubble pile, overlain by a substantial regolith layer; the large concavities would represent giant impact basins, formed by events close to the catastrophic break–up threshold. This interpretation is consistent with our models, in particular those including a significant ejecta velocity vs. mass dependence, as they show that even for bodies as small as Gaspra a large fraction of the material ejected after impacts can be reaccumulated by self–gravity both in the shattering and in the cratering regime (see Figs. 10–12). Thus Gaspra may have been originated in a shattering event followed by the reaggregation of a few large blocks; the subsequent formation of some giant craters may have produced the surface regolith and erased the small–scale topography.

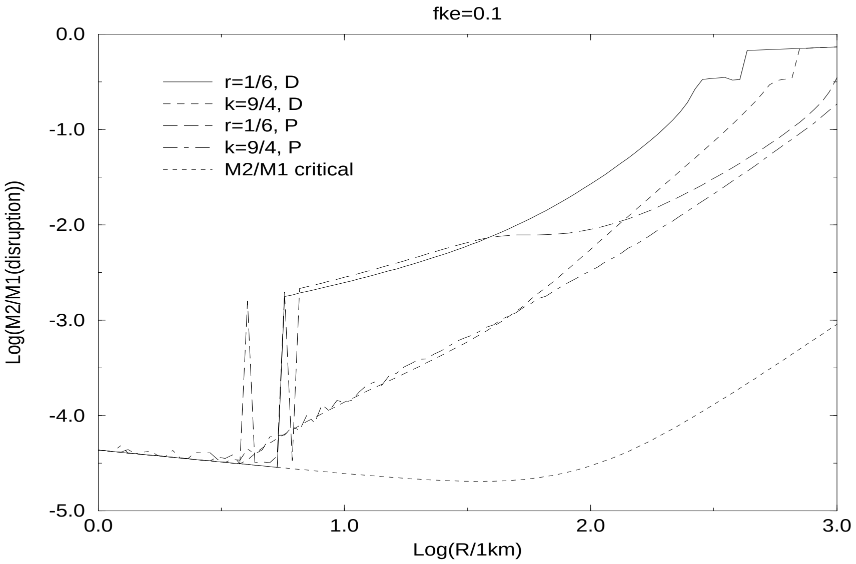

Fig. 13: The critical mass ratio for *disruption* versus the logarithm of the target size, for the four models used in the previous figures. The bottom (dashed) line is the threshold mass ratio for *fragmentation*.

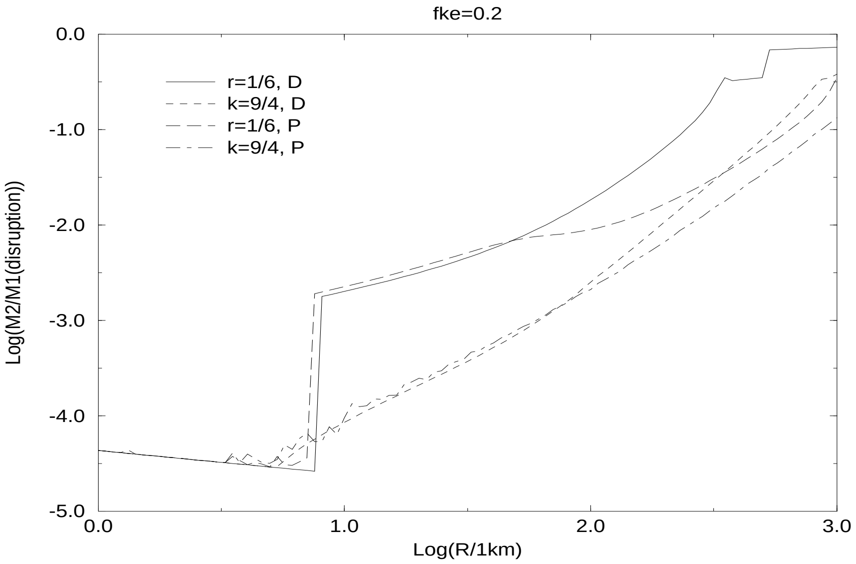

Fig. 14: The same as Fig. 13, but with $f_{ke} = 0.2$.

Figs. 13 and 14 show another type of diagram, which should be compared with Fig. 5 of Davis *et al.* (1985) and Fig. 5 of Housen and Holsapple (1990). Here the lower (dashed) curve corresponds to the critical projectile–to–target mass ratio for fragmentation, which is a function of size because of the strength scaling relationship (1). The other curves give the threshold mass ratio for collisional disruption, with one half of the target mass dispersed to infinity. While for small asteroids, whose gravity is not efficient in reaccumulating fragments, the fragmentation and disruption thresholds coincide, for asteroids $\approx 100\,km$ across there is a large gap between the two thresholds, due to the gravitational reaccumulation process. In this case, the curves show that the for the $r = 1/6$ models a sudden discontinuity appears when a critical size is exceeded, while for the $k = 9/4$ case there is a more gradual transition. This behaviour can be explained as follows: in the $k = 9/4$ case, when all the fragment velocities are close to each other, a modest specific energy (i.e., mass ratio) increase may be enough to exceed V_{esc}; on the other hand, in the $r = 1/6$ case, after self–gravity has become strong enough to reaccumulate the largest fragments, a moderate increase in the specific energy causes a mass shift to fragments of smaller sizes, which receive a larger fraction of the available energy, thus preventing the largest fragments from starting faster (and being able to escape).

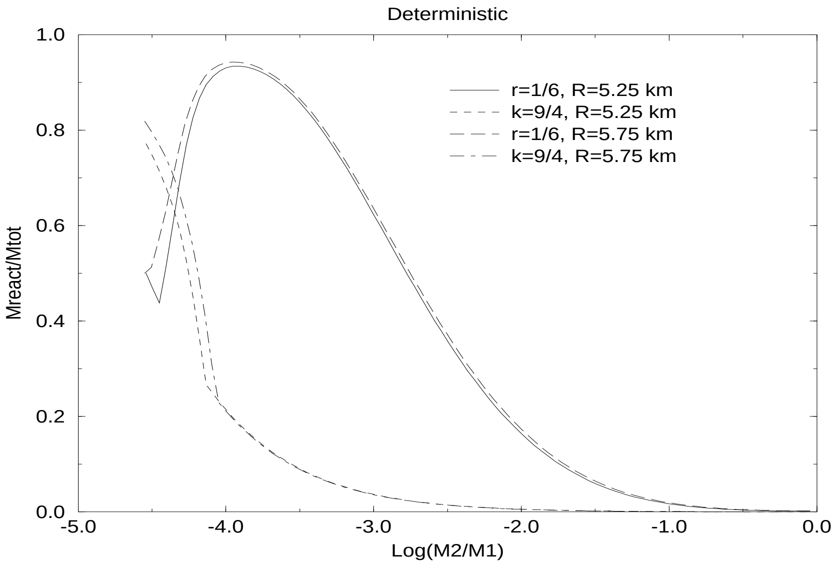

Fig. 15: The reaccumulated mass fraction versus M_2/M_1 for the deterministic $r = 1/6$ and $k = 9/4$ models and for two values of the target radius, close to each other but on the two sides of the critical value for which reaccumulation starts to be effective.

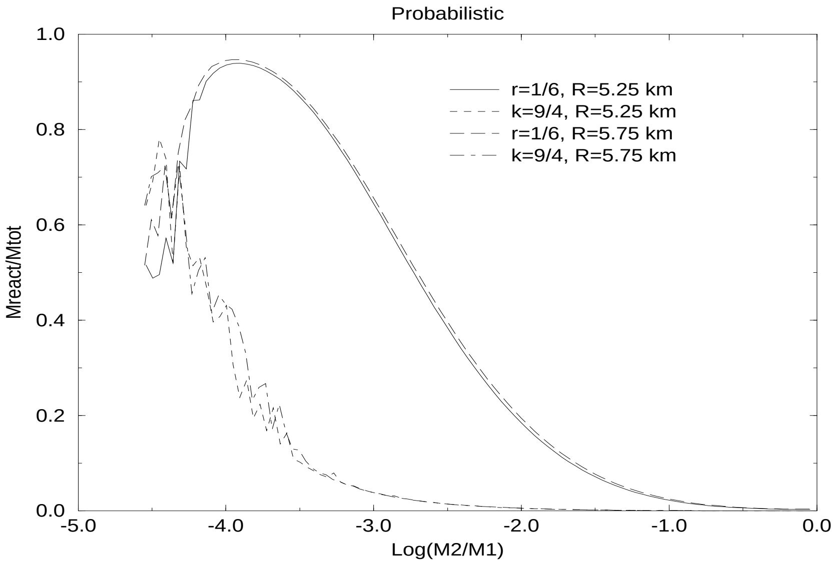

Fig. 16: The same as Fig. 15 but for the probabilistic models.

This sudden "runaway reaccumulation" phenomenon in the $r = 1/6$ models is illustrated in Figs. 15 and 16. Here the reaccumulated mass fraction is plotted versus M_2/M_1 for two values of the target radius, close to each other but on the two sides of the critical value. While with the $k = 9/4$ model the reaccumulated mass always decreases in a nearly–monotonic way when the impact gets more energetic, the opposite happens with the $r = 1/6$ model: for the lower size, when the fragmentation threshold is exceeded by a small amount, there is still a small drop of the reaccumulated mass fraction to values $< 1/2$, but this drop disappears at the larger size, since in this case more energetic collisions result initially into more effective reaccumulation; only for much higher mass ratios the reaccumulated fraction decreases, falling again below $1/2$ only for values of M_2/M_1 exceeding the fragmentation threshold by almost two orders of magnitude.

This is just an example of what we believe is an important finding of this work: for asteroidal–sized bodies, even keeping fixed the (poorly known) parameter f_{ke}, the predicted collisional outcomes depend in a sensitive way on the adopted fragment velocity vs. mass model. Take for instance the formation of an asteroid family from a target $\approx 200\,km$ across, which requires a collisional event capable of ejecting to infinity a substantial fraction of the mass of the parent body. Fig. 13 shows that, even keeping $f_{ke} = 0.1$ and limiting ourselves to the four models described earlier, the required projectile–to–target mass ratio ranges from about $1/300$ ($k = 9/4$, probabilistic) to $1/30$ ($r = 1/6$, deterministic), implying a projectile diameter between 30 km and 65 km. This entails about a factor 4 of uncertainty in the available number of projectiles ($\approx$ 1100 versus 300, respectively; see Fig. 3 of Cellino *et al.*, 1991), with a similar uncertainty in the collision lifetimes and therefore in the expected number of families. With the average collision rate derived by Farinella and Davis (1992; see Sec. 1) and the current population of main–belt asteroids, the expected number of disrupted 200 km–sized parent bodies may range between 1.5 and 5. The agreement with the results of family searches such as that of Zappalà *et al.* (1990) is good, but reducing the uncertainty would be very important.

7 Conclusions and future work

The algorithm described in this paper is simple enough to be applied in a quick and effective way to a variety of studies on the collisional evolution of small solar system bodies. In Sec. 6 we have presented some examples related to the evolution of asteroids and the origin of asteroid families, but similar analyses — with comparable resulting uncertainties — could be performed for other cases of catastrophic or nearly–catastrophic impacts occurred in the solar system. A list might include: the formation of Vesta's family from a giant crater preserving intact most of the basaltic crust of this asteroid (Davis *et al.*, 1985; Rosa *et al.*, 1992); the collisional origin of the dust bands discovered by IRAS (Sykes *et al.*, 1989); the formation of reaccumulated, rapidly spinning (or binary) asteroids (Farinella *et al.*, 1982, 1985; Weidenschilling *et al.*, 1989); the origin of very large craters and impact basins observed on many natural satellites (Chapman and McKinnon, 1986); the collisional disruption of Hyperion (Farinella *et al.*, 1983); the formation of planetary rings from disrupted satellites (Harris, 1984).

Of course, many input parameters of the collisional models — and also the validity of several empirical relationships used in Secs. 2 to to 6 — are still subject to considerable uncertainty. We are confident that this uncertainty will be reduced in the near future as result of the combination between further laboratory experiments and complex numerical simulations of the collisional disruption process. We think that the algorithm presented here is simple and flexible enough to easily incorporate new theoretical and experimental results. Once this is done, the output of our code can be written as a three–dimensional matrix, specifying how many objects end up in the i–th mass bin following a collision between two bodies lying in the j-th and k–th mass bins. This matrix can then be read by a program aimed at simulating the time evolution of an initial asteroid (or planetesimal, or planetary ring particle) population by computing in any time step for every pair of mass bins the expected number of collisions, as in the work of Greenberg *et al.* (1978), Davis *et al.* (1979, 1985, 1989), and Farinella *et al.* (1992). We are going to present in a forthcoming paper some results on the sensitivity of the outcomes of the simulated asteroid collisional evolution (in terms of the observable size distribution), with respect to the fragment velocity vs. mass correlation models, as discussed in Sec. 6, and other poorly known input parameters. We also plan to develop in the future, along the same lines discussed here, a more comprehensive algorithm capable of computing impact outcomes, not only in terms of sizes but also including spins, i.e., angular momenta of rotation — for the physics involved in this problem see Davis *et al.* (1989), Cellino *et al.* (1990) and Farinella *et al.* (1992).

Acknowledgments

We are grateful to the reviewer R. Greenberg for pointing to us the recent hydrocode modelling work, and to A. Campo Bagatin, A. Cellino, D.R. Davis, G. Martelli, P. Paolicchi and V. Zappalà for useful discussions and comments. J.–M. Petit's stay in Pisa in 1991 was supported through the CNRS–CNR researcher exchange agreement. P. Farinella acknowledges financial support by the Observatoire de la Côte d'Azur and the EEC research grant no. SC1–0011–C(GDF).

References

[1] Asphaug, E., Benz, W., & Melosh, H.J., 1992. *Asteroid impact studies with SPH 3D (abstract).* Bull. Amer. Astr. Soc., in press,

[2] Belton, M.J.S., Veverka, J., Thomas, P., Helfenstein, P., Simonelli, D., Chapman, C., Davies, M.E., Greeley, R., Greenberg, R., Head, J., Murchie, S., Klaasen, K., Johnson, T.V., McEwen, A., Morrison, D., Neukum, G., Fanale, F., Anger, C., Carr, M., Pilcher, C., 1992. *Galileo encounter with 951 Gaspra: First pictures of an asteroid.* Science **257**, pp. 1647––1652.

[3] Cellino, A., Zappalà, V., Davis, D.R., Farinella, P., & Paolicchi, P., 1990. *Asteroid collisional evolution, I. Angular momentum splash: Despinning asteroids through catastrophic collisions.* Icarus **87**, pp. 391––402.

[4] Cellino, A., Zappalà, V., & Farinella, P., 1991. *The size distribution of main–belt asteroids from IRAS data.* Mon. Not. R. astr. Soc. **253**, pp. 561––574.

[5] Chapman, C.R., & McKinnon, W.B., 1986. *Cratering on planetary satellites.* in *Satellites,* eds. J.A. Burns and M.S. Matthews, Univ. of Arizona Press, pp. 492––580.

[6] Chapman, C.R., Paolicchi, P., Zappalà, V., Binzel, R.P, & Bell, J.F., 1989. *Asteroid families: Physical properties and evolution.* in *Asteroids II,* eds. R.P. Binzel, T. Gehrels & M.S. Matthews, Univ. of Arizona Press, pp. 386––415.

[7] Davis, D.R., 1990. *On social disintegration in the solar system: The disruption of families.* presented at the Third International Workshop on Catastrophic Disruption of Small Solar System Bodies (Kyoto, Japan, September 1990).

[8] Davis, D.R., Chapman, C.R., Greenberg, R., & Harris, A.W., 1979. *Collisional evolution of asteroids: Populations, rotations, and velocities.* in *Asteroids,* ed. T. Gehrels, Univ. of Arizona Press, pp. 528––557.

[9] Davis, D.R., Chapman, C.R., Weidenschilling, S.J., & Greenberg, R., 1985. *Collisional history of asteroids: Evidence from Vesta and the Hirayama families.* Icarus **62**, pp. 30––53.

[10] Davis, D.R., Farinella, P., Paolicchi, P., & Zappalà, V. (eds.), 1986. *Catastrophic Disruption of Asteroids and Satellites.* J. Ital. Astron. Soc. **57**, n. 1.

[11] Davis, D.R., Farinella, P., Paolicchi, P., Weidenschilling, S.J., & Binzel, R.P., 1989. *Asteroid collisional history: Effects on sizes and spins.* in *Asteroids II,* eds. R.P. Binzel, T. Gehrels & M.S. Matthews, Univ. of Arizona Press, pp. 805––826.

[12] Davis, D.R., & Ryan, E.V., 1990. *On collisional disruption: Experimental results and scaling laws.* Icarus **83**, pp. 156––182.

[13] Dobrovolskis, A., & Burns, J.A., 1984. *Angular momentum drain: A mechanism for despinning asteroids.* Icarus **57**, pp. 464––476.

[14] Farinella, P., Paolicchi, P., & Zappalà, V., 1982. *The asteroids as outcomes of catastrophic collisions.* Icarus **52**, pp. 409––433.

[15] Farinella, P., Milani, A., Nobili, A.M., Paolicchi, P., & Zappalà, V., 1983. *Hyperion: Collisional disruption of a resonant satellite.* Icarus **54**, pp. 353––360.

[16] Farinella, P., Paolicchi, P., & Zappalà, V., 1985. *Original abundance of asteroids from their present rotational properties.* Mon. Not. R. astr. Soc. **216**, pp. 565––570.

[17] Farinella, P., Paolicchi, P., Cellino, A., & Zappalà, V., 1988. *Escape velocity for fragments of collisionally shattered solar system bodies.* Bull. Obs. Astron. Belgrade **138**, pp. 88––90.

[18] Farinella, P., & Davis, D.R., 1992. *Collision rates and impact velocities in the main asteroid belt.* Icarus **97**, pp. 111––123.

[19] Farinella, P., Davis, D.R., Paolicchi, P., Cellino, A., & Zappalà, V., 1992. *Asteroid collisional evolution: An integrated model for the evolution of asteroid rotation rates.* Astron. Astrophys. **253**, pp. 604––614.

[20] Fujiwara, A., Kamimoto, G., & tsukamoto, A., 1977. *Destruction of basaltic bodies by high–velocity impact.* Icarus **31**, pp. 277––288.

[21] Fujiwara, A., & Tsukamoto, A., 1980. *Experimental study on the velocity of fragments in collisional breakup.* Icarus **44**, pp. 142––153.

[22] Fujiwara, A., Cerroni, P., Davis, D.R., Ryan, E., Di Martino, M., Holsapple, K., & Housen, K., 1989. *Experiments and scaling laws on catastrophic collisions.* in *Asteroids II,* eds. R.P. Binzel, T. Gehrels & M.S. Matthews, Univ. of Arizona Press, pp. 240––265.

[23] Gault, D.E., Shoemaker, E.M., & Moore, H.J., 1963. *Spray ejected from the lunar surface by meteoroid impact.* NASA Tech. Note **D–1767**,

[24] Greenberg, R., Wacker, J.F., Hartmann, W.K., & Chapman, C.R., 1978. *Planetesimals to planets: Numerical simulation of collisional evolution.* Icarus **35**, pp. 1––26.

[25] Greenberg, R., Nolan, M.C., Bottke, W.F., Kolvoord, R.A., Veverka, J., & the Galileo imaging team, 1992. *Collisional and dynamical evolution of Gaspra (abstract).* Bull. Amer. Astr. Soc., in press,

[26] Harris, A.W., 1984. *The origin and evolution of planetary rings.* in *Planetary Rings,* eds. R. Greenberg & A. Brahic, Univ. of Arizona Press, pp. 641––659.

[27] Hartmann, W.K., 1969. *Terrestrial, lunar and interplanetary rock fragmentation.* Icarus **10**, pp. 201––213.

[28] Hartmann, W.K., 1988. *Impact strength and energy partitioning in impacts into finite solid targets.* Lunar Planet. Sci. **XIX**, pp. 451-–452.

[29] Housen, K.R., & Holsapple, K.A., 1990. *On the fragmentation of asteroids and planetary satellites.* Icarus **84**, pp. 226–253.

[30] Housen, K.R., Schmidt, R.M., & Holsappple, K.A., 1991. *Laboratory simulations of large scale fragmentation events.* Icarus **94**, pp. 180-–190.

[31] Kresàk, Ľ., 1977. *Mass content and mass distribution in the asteroid system.* Bull. Astron. Inst. Czech. **28**, pp. 65-–82.

[32] Nakamura, A., & Fujiwara, A., 1991. *Velocity distribution of fragments formed in a simulated collisional disruption.* Icarus **92**, pp. 132-–146.

[33] Nolan, M.C., Asphaug, E., & Greenberg, R., 1992. *Numerical simulation of impacts on small asteroids (abstract).* Bull. Amer. Astr. Soc., in press,

[34] Öpik, E.J., 1951. *Collision probabilities with the planets and the distribution of interplanetary matter.* Proc. Royal Irish Acad. **54A**, pp. 164-–199.

[35] Ostro, S.J., Chandler, J.F., Hine, A.A., Rosema, K.D., Shapiro, L.L., & Yeomans, D.K., 1990. *Radar images of asteroid 1989 PB.* Science **248**, pp. 1523-–1528.

[36] Paolicchi, P., Cellino, A., Farinella, P., & Zappalà, V., 1989. *A semiempirical model of catastrophic breakup processes.* Icarus **77**, pp. 187-–212.

[37] Paolicchi, P., Verlicchi, A., & Cellino, A., 1992. *A new semiempirical model for catastrophic impact processes (abstract).* Bull. Amer. Astr. Soc., in press,

[38] Piotrowski, S.I., 1953. *The collisions of asteroids.* Acta Astron. Ser. A **6**, pp. 115-–138.

[39] Rosa, F., Cellino, A., Zappalà, V., & Farinella, P., 1992. *Crater ejecta from Vesta.* in preparation

[40] Ryan, E.V., Asphaug, E., & Melosh, H.J., 1990. *Hydrocode predictions of collisional outcomes: Effects of target size.* Lunar Planet. Sci. **XXI**, pp. 1155-–1156.

[41] Ryan, E.V., & Melosh, H.J., 1992. *Understanding asteroid collisions: The effect of target size on collisional outcome (abstract).* Bull. Amer. Astr. Soc., in press,

[42] Stöffler, D., Gault, D.E., Wedekind, J., and Polkowski, G., 1975. *Experimental hypervelocity impacts into quartz sand: Distribution and shock metamorphism of ejecta.* J. Geophys. Res. **80**, pp. 4062––4077.

[43] Sykes, M.V., Greenberg, R., Dermott, S.F., Nicholson, P.D., and Burns, J.A., 1989. *Dust bands in the asteroid belt.* in *Asteroids II,* eds. R.P. Binzel, T.Gehrels & M.S.Matthews, Univ. of Arizona Press, pp. 336––367.

[44] Weidenschilling, S.J., Paolicchi, P., & Zappalà, V., 1989. *Do asteroids have satellites?.* in *Asteroids II,* eds. R.P.Binzel, T.Gehrels and M.S.Matthews, Univ. of Arizona Press, pp. 643––658.

[45] Zappalà, V., Farinella, P., Knežević, Z., & Paolicchi, P., 1984. *Collisional origin of asteroid families: Mass and velocity distributions.* Icarus **59**, pp. 261–285.

[46] Zappalà, V., Cellino, A., Farinella, P., & Kneževiĉ, Z., 1990. *Asteroid families. I. Identification by hierachical clustering and reliability assessment.* Astron. J. **100**, pp. 2030––2046.